Mechanical Systems and Signal Processing 229 (2025) 112487

Contents lists available at ScienceDirect

Mechanical Systems and Signal Processing

journal homepage: www.elsevier.com/locate/ymssp

Dynamic substructuring-based identification of the rivet-squeezing force

Tim Vrtač, Miha Kodrič, Miha Pogačar, Gregor Čepon *

Faculty of Mechanical Engineering, University of Ljubljana, Aškerčeva 6, 1000 Ljubljana, Slovenia

ARTICLE INFO

Communicated by M. Brake

Keywords:
Rivet
Rivet-squeezing force
Joint identification
Dynamic substructuring
Quality control

ABSTRACT

Riveting, which involves the plastic deformation of a rivet to join components, is widely used in automotive, aerospace, and construction due to its simplicity, reliability, and ease of disassembly. Ensuring high-quality products requires End-of-Line testing of riveted joints, typically using non-destructive methods like ultrasonic testing. However, these methods do not enable the evaluation of the rivet-squeezing force, which significantly impacts the integrity and dynamic properties of the riveted joint. In this paper, an approach to indirectly evaluate the rivet-squeezing force through the identification of the joint's dynamic properties is proposed. Using Frequency-Based Substructuring, the joint's dynamics are decoupled from the structural assembly, isolating the influence of the squeezing force solely to the riveted joint and not the whole assembly. This method allows for the construction of a dataset of isolated joint impedances correlated with specific rivet-squeezing forces, serving as a reference dataset. The uniqueness of the proposed approach lies in its operation on joint impedances—the joint for which the squeezing force is to be determined does not need to originate from the same assembly as the dataset joints. For a structure of interest with an unknown squeezing force, the joint's impedance is first obtained using the FBS decoupling approach. This impedance is then characterized by comparison with the reference dataset impedances to deduce the squeezing force based on a classification procedure. It is demonstrated that the proposed approach can be used to classify the rivet-squeezing force for the structure of interest and can thus be applied in the End-of-Line control of riveted joints. The proposed approach is limited only with requirement that the riveted joints share similarities in terms of material and geometry near the joints.

1. Introduction

Riveting, a method of joining metal sheets, is based on the plastic deformation of the rivet. Due to the simplicity of the process, the ease of disassembly, and the high reliability [1] it is commonly used in applications like aerospace, civil construction, and the automotive industry [2]. The method has advantages that contribute to its widespread applicability, e.g., the possibility to join combinations of dissimilar materials and its lack of susceptibility to loosening when exposed to dynamic loads (which can occur with bolted joints) [3]. Riveting also allows us to join light alloys more easily than with resistance spot welding (which can be difficult due to a high thermal conductivity, a low melting point, etc.) [4].

* Corresponding author.
E-mail address: gregor.cepon@fs.uni-lj.si (G. Čepon).

https://doi.org/10.1016/j.ymssp.2025.112487
Received 30 July 2024; Received in revised form 30 December 2024; Accepted 17 February 2025

Available online 1 March 2025

Reliable, high-quality products must meet requirements relating to fatigue life and strength. As inter-component connections, i.e., joints, have an impact on performance, and even the survivability of an assembled system [5], there are demands for better-quality riveted joints. A complex set of parameters affects the properties of a riveted joint, and so numerous studies have been undertaken to identify these parameters and their effects. Wang et al. [6] studied the effect of the rivet-squeezing force, the length of the rivet, the tolerance of the rivet's diameter and the tolerance of the hole made for the rivet on the dimensions of the riveting head. In their paper, Li et al. [7] experimentally tested the effect of the rivet-squeezing force and the riveting-die configuration on the fatigue life of the assembly. It was shown by Zhang [8], that when multiple rivets are applied, the riveting sequence and direction affect the stress distribution within the joint. Of these parameters, the rivet-squeezing force is one of the most commonly studied. Müller [9] studied the effects of the squeezing force on the filling of the rivet hole, the size of the driven head, and the residual stresses in the assembly. Li et al. [10] performed an experimental study to analyze the effects of the squeezing force on the structural integrity of the joint under different loading conditions and on the failure modes of the riveted joint. Zeng et al. [11] showed that within the allowable range, increasing the squeezing force extends the fatigue life of the riveted joint (at excessive forces the fatigue life starts decreasing anew). In their study, Huan and Lui [12] numerically and experimentally investigated how the magnitude of the squeezing forces affects the residual stresses around the hole made for the rivet. Due to its considerable effect on the dynamic properties of joints, and with this on the fatigue life of the product, as well as on its loading capabilities, the identification of the squeezing force is very important.

In the manufacturing process, variations in the applied squeezing force can occur for multiple reasons, e.g., incorrect tool setting, insufficient pressure in pneumatic/hydraulic systems, wear of riveting tools, etc. Due to these variations, it is reasonable to implement End-of-Line (EoL) control for the riveted joint at key locations, i.e., at highly loaded locations, or locations where the joint directly affects the functionality of the product [13–16].

There are a variety of methods that allow us to test different aspects of a riveted joint's quality (fatigue life, mechanical strength, etc.). These methods can be divided into destructive and non-destructive. Destructive tests provide us with information such as the tensile and shear strength of the joint (tensile and shear tests [17]), or fatigue strength of the joint (fatigue test [18]). The drawback of this kind of testing is that samples are demolished during the test. However, when performing EoL control in the manufacturing process, non-destructive testing is the only feasible option. These methods commonly allow us to detect defects in a material on the surface of the structure (dye-penetrant inspection) or even inside the material (ultrasonic testing [19,20], pulse thermography [21], etc.). However, non-destructive tests usually do not enable a direct evaluation of the joint's dynamics properties, in particular with respect to the rivet-squeezing force. In accordance with previous research (e.g. by Li et al. [7], Müller [9], Li et al. [10], Huan and Lui [12], etc.), regulating the rivet-squeezing force allows us to control the residual stresses, the structural integrity, and the expected fatigue life of the joint. In various studies [9,11,12], it was demonstrated that the riveting squeezing force is in direct correlation with the dynamic properties of joints. Therefore, a joint's rivet-squeezing force can be characterized indirectly, by identifying the dynamic properties of the assembly (such as natural frequencies, mode shapes, etc.). Consequently, by identifying the variations in the dynamic properties of the assembly, it is possible to indirectly estimate the squeezing force. However, this approach is limited to the particular assembly for which the initial identification of the influence of the squeezing force on dynamic properties was conducted. For modified assemblies or different systems, this identification process must be entirely repeated, which makes it impractical.

In this paper, we propose a new, more general method that aims to identify the squeezing force by examining the dynamic properties of the riveted joint, rather than analyzing the entire assembly. Since the identification process relies on the dynamic properties of the isolated riveted joint, it can be used to evaluate the squeezing force on a modified structure or an entirely different assembly. The only requirement is that the riveted joints share similarities in terms of material and geometry near the joints. This approach utilizes the methodology of Frequency-Based Substructuring (FBS), which allows for the decoupling joint-adjacent components from the dynamic response of the assembled system [22], thereby identifying the influence of the squeezing force on the joint's dynamics alone. An important advantage of the identified dynamic model of the riveted joint is that the calibrated model is transferable to different assembled systems; i.e., it can be used to identify the squeezing force of different assemblies. Kreutz et al. [23] demonstrated this approach to characterize the dynamics of bolted joints; however, here we are extending it for riveting squeezing force identification. Estimating the joint's quality based on its dynamic response brings another significant benefit. Due to the variations in the manufacturing process (e.g. variations in the rivet or metal sheet plate material, incorrect tool setting, wear of the riveting tool, etc.), the dynamic response of the riveted joint can vary substantially despite the same squeezing force being considered during the riveting process. When evaluating the squeezing force corresponding to the riveted joint of interest based on its dynamic properties (joint admittance), these inconsistencies directly influence the dynamic response of the joint. Thus the indirectly estimated squeezing force based on joint admittance gives us much better information regarding the quality of each joint than the sole measurement of the force during the manufacturing process. Consequently, the proposed approach not only ensures a reliable evaluation of joint squeezing force but also enables the estimation of joint consistency over its lifetime, due to the indirect estimation of squeezing force based on the joint's experimental response model that can be obtained by measuring the response model of entire structure.

The idea in this study relies on obtaining the riveted joint's impedances using the FBS decoupling approach on a laboratory structure, for which the rivet-squeezing force is measured during the riveting process. In this way, it is possible to construct a dataset of isolated joint impedances that are correlated with specific riveting squeezing forces and serve as a reference dataset. For the structure of interest, for which the squeezing force is unknown, the joint's impedance is first obtained using the FBS decoupling approach. This impedance is characterized by comparison with the reference dataset impedance of the riveted joints for which the force is known. The uniqueness of the proposed approach lies in the fact that it operates on joint impedance—the joint for which

the squeezing force is to be determined does not need to originate from the same assembly as the dataset joints. The squeezing force for the joint of interest is then determined by characterizing the coherence between the isolated joint's impedance of the reference dataset and the structure of interest. It is demonstrated that this approach can effectively classify the rivet-squeezing force for the structure of interest and, consequently, evaluate the quality of the riveted joints.

The paper is structured as follows. Section 2 focuses on how the model of the riveted joint is obtained using the FBS-based approach. This is followed by a detailed description of the properties of the resulting joint model. In Section 3 we elaborate on the procedure for the squeezing-force identification. In Section 4, the proposed approach is demonstrated in a laboratory example that is used to create a joint dataset. This dataset is then employed to identify the rivet-squeezing force for three validation samples. Finally, the conclusions are presented.

2. Characterization of a riveted joint

The approach of extracting the riveted-joint model from the dynamic model of the assembled system requires the dynamic decoupling of multiple system components (i.e., substructures) using the FBS approach. Therefore, first, the FBS will be briefly introduced,[1] followed by a description of the joint-characterization process and the details regarding the resulting joint model.

2.1. Frequency-based substructuring

FBS allows us to analyze complex systems based on the dynamic properties of their constituent parts. Each part is described by the corresponding admittance matrix $\mathbf{Y}^i(\omega)$.[2] By treating each substructure of the system individually, it is possible to describe the response of the system with the following set of equations[3]:

$$\boldsymbol{u} = \mathbf{Y}(\boldsymbol{f} + \boldsymbol{g}), \tag{1}$$

where $\boldsymbol{u}$ is a vector of responses (e.g., displacements), $\mathbf{Y}$ is an uncoupled admittance matrix of the system, consisting of block-diagonally placed admittance matrices of the substructures ($\mathrm{diag}([\mathbf{Y}^1, \mathbf{Y}^2, \dots, \mathbf{Y}^n])$, where n is the number of substructures in the system), $\boldsymbol{f}$ is a vector of external loads and $\boldsymbol{g}$ is a vector of interface loads. The interface loads $\boldsymbol{g}$ are the forces and moments at the interface between substructures, holding substructures together (Fig. 1a). For the case presented in Fig. 1a, terms from Eq. (1) can be written as follows:

$$\boldsymbol{u} = \begin{Bmatrix} \boldsymbol{u}_1^{\mathrm{A}} \\ \boldsymbol{u}_2^{\mathrm{A}} \\ \boldsymbol{u}_2^{\mathrm{B}} \\ \boldsymbol{u}_3^{\mathrm{B}} \end{Bmatrix}, \quad \mathbf{Y} = \begin{bmatrix} \mathbf{Y}^{\mathrm{A}} & \mathbf{0} \\ \mathbf{0} & \mathbf{Y}^{\mathrm{B}} \end{bmatrix}, \quad \boldsymbol{f} = \begin{Bmatrix} \boldsymbol{f}_1^{\mathrm{A}} \\ \mathbf{0} \\ \mathbf{0} \\ \mathbf{0} \end{Bmatrix}, \quad \boldsymbol{g} = \begin{Bmatrix} \mathbf{0} \\ \boldsymbol{g}_2^{\mathrm{A}} \\ \boldsymbol{g}_2^{\mathrm{B}} \\ \mathbf{0} \end{Bmatrix}, \tag{2}$$

where subscript $\star_1$ denotes internal DoFs corresponding to substructure A, subscript $\star_2$ DoFs at the interface between both substructures (i.e. interface DoFs), and subscript $\star_3$ internal DoFs corresponding to substructure B.[4]

The definition of the uncoupled admittance $\mathbf{Y}$ in Eq. (2) is intended for dynamic coupling of substructures A and B into assembly AB (Fig. 1b). Besides dynamic coupling, FBS allows us to decouple one or more substructures from the assembled system (e.g. in Fig. 1c substructure B is decoupled from assembly AB). This can be achieved by inserting negative admittances of the substructures to be decoupled into the uncoupled admittance $\mathbf{Y}$. For the case in Fig. 1c, $\mathbf{Y}$ is structured as follows [27]:

$$\mathbf{Y} = \begin{bmatrix} \mathbf{Y}^{\mathrm{AB}} & \mathbf{0} \\ \mathbf{0} & -\mathbf{Y}^{\mathrm{B}} \end{bmatrix}. \tag{3}$$

To obtain information about the decoupled system, two conditions must be enforced. The first one is the compatibility condition, which stipulates matching responses at the interfaces between pairs of adjacent substructures:

$$\mathbf{B}_{\mathrm{c}}\boldsymbol{u} = \mathbf{0}; \quad \mathbf{B}_{\mathrm{c}} = \begin{bmatrix} \mathbf{0} & \mathbf{I} & -\mathbf{I} & \mathbf{0} \end{bmatrix}, \tag{4}$$

where $\mathbf{B}_{\mathrm{c}}$ is a Boolean matrix, connecting pairs of interface response DoFs.

The second condition to be enforced is an equilibrium condition, which imposes an equilibrium of interface forces between pairs of adjacent substructures:

$$\mathbf{B}_{\mathrm{e}}^{\mathrm{T}}\boldsymbol{\lambda} = \boldsymbol{g}; \quad \mathbf{B}_{\mathrm{e}} = \begin{bmatrix} \mathbf{0} & \mathbf{I} & -\mathbf{I} & \mathbf{0} \end{bmatrix}, \tag{5}$$

[1] The interested reader is referred to Refs. [24–27] where the details regarding FBS are further elaborated.

[2] Admittance matrix $\mathbf{Y}(\omega)$ is a matrix, containing Frequency Response Functions (FRFs) connecting selected excitation and response degrees of freedom (DoFs) of the structure.

[3] An explicit dependency on the frequency is omitted to improve the readability of the notation, as will be the case for the remainder of the paper.

[4] Interface DoFs are DoFs located at the boundary between the substructures, while internal DoFs denote the DoFs of substructures located away from the interface.

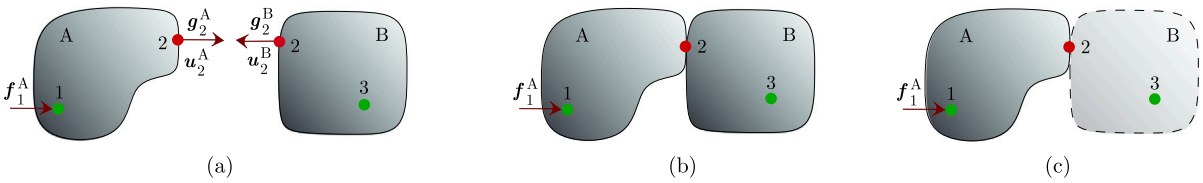

Fig. 1. Dynamic substructuring: (a) Uncoupled system of substructures A and B, (b) coupled system of substructures A and B, and (c) decoupling of substructure B from assembly AB. (●) Interface DoFs, (●) internal DoFs.

where $\mathbf{B}_e$ is a Boolean matrix connecting pairs of interface excitation DoFs, and $\boldsymbol{\lambda}$ is a vector of Lagrange multipliers denoting the magnitude of each pair of interface forces (e.g., for interface forces between adjacent substructures A and B, $\lambda_2 = g_2^A = -g_2^B$).

Imposing Eqs. (4) and (5) on a system of Eqs. (1), a system of equations for the coupled system can be derived:

$$\boldsymbol{u} = \widetilde{\mathbf{Y}}\boldsymbol{f}, \tag{6}$$

$\widetilde{\mathbf{Y}}$ being an admittance matrix of the decoupled system, defined by the equation, often referred to as the Lagrange Multiplier Frequency-Based Substructuring (LM FBS) equation [25]:

$$\widetilde{\mathbf{Y}} = \mathbf{Y} - \mathbf{Y}\mathbf{B}_e^T \left(\mathbf{B}_c\mathbf{Y}\mathbf{B}_e^T\right)^{-1} \mathbf{B}_c\mathbf{Y}. \tag{7}$$

There are two techniques of dynamic decoupling. The first one is a standard interface technique, which means that only interface DoFs ($\star_2$ in Fig. 1c) are used in the compatibility and equilibrium conditions (Eqs. (4) and (5), respectively). The drawback of this approach is that spurious peaks can occur in the resulting FRFs [28], which are a consequence of the residual dynamics of the original system, not observed and/or controlled in the interface DoFs [29]. Besides that, when dealing with experimentally obtained FRFs, presence of measurement errors is inevitable. In the process of standard decoupling, small discrepancies between the measured FRFs and the actual FRFs for the excitation and response DoF of interest get severely amplified, resulting in flawed results [30]. These effects can be alleviated by extending a set of DoFs to be decoupled to the internal DoFs of the decoupled component ($\star_3$ in Fig. 1c). This approach is referred to as extended interface decoupling [31]. In the process of extended interface approach, compatibility condition is enforced on the internal DoFs of the decoupled component for which compatibility is satisfied a priori. Therefore, these FRFs provide no new information in the case where FRFs contain no errors or noise. However, since some measurement errors are always present, adding extra set of DoFs provides additional information an thus helps reducing the impact of these errors [27,31].

Due to the reasons mentioned above, interface matrix $\mathbf{B}_c\mathbf{Y}\mathbf{B}_e^T$ is prone to being ill-conditioned, which causes problems during calculating the interface matrix inverse in LM FBS Eq. (7). In order to tackle this problem, Lim and Li [32] proposed the use of truncated singular value decomposition (TSVD). Since then the potential of this approach to improve the results of dynamic coupling has been demonstrated in various studies [31,33,34]. During TSVD the interface matrix is decomposed into a matrix of left singular vectors, a diagonal matrix containing singular values, and a matrix of right singular vectors. Close-to-zero singular values and corresponding left and right singular vectors are then truncated. The truncated matrices are then used in a Moore–Penrose matrix inverse which gives us the inverse of the interface matrix $\left(\mathbf{B}_c\mathbf{Y}\mathbf{B}_e^T\right)^+$ [34,35].[5]

2.2. Obtaining a riveted-joint model

To perform rivet characterization using the FBS-based approach [22], three models are needed: a model of the assembled system $\mathbf{Y}^{ARB}$ and two models of the plates joined by the rivet $\mathbf{Y}^A$ and $\mathbf{Y}^B$ (Fig. 2). For the purpose of obtaining the admittance matrix of the riveted joint $\mathbf{Y}^R$, $\mathbf{Y}^A$ and $\mathbf{Y}^B$ will be decoupled from $\mathbf{Y}^{ARB}$. This can be done by using the LM FBS Eq. (7) with the global admittance matrix defined as follows:

$$\mathbf{Y} = \begin{bmatrix} \mathbf{Y}^{ARB} & \mathbf{0} & \mathbf{0} \\ \mathbf{0} & -\mathbf{Y}^A & \mathbf{0} \\ \mathbf{0} & \mathbf{0} & -\mathbf{Y}^B \end{bmatrix}. \tag{8}$$

Matrix $\widetilde{\mathbf{Y}}$ resulting from the Eq. (7) contains all the DoFs of ARB, and both substructures A and B (with some DoFs duplicated). As the substructures A and B have been decoupled from the assembly, elements of $\widetilde{\mathbf{Y}}$, for which response DoF or excitation DoF (or both) belong to internal DoFs of substructures A or B, have no physical meaning. What we would like to obtain, is the admittance of the riveted joint $\mathbf{Y}^R$ containing only excitation and response DoFs belonging to the riveted joint R (Fig. 2). To achieve this, the needed part of $\widetilde{\mathbf{Y}}$ can be extracted by using the following equation:

[5] $\mathbf{B}_c\mathbf{Y}\mathbf{B}_e^T = \mathbf{U}\boldsymbol{\Sigma}\mathbf{V}^H$, where $\mathbf{U} \in \mathbb{C}^{m\times m}$ is a matrix of left singular vectors, $\boldsymbol{\Sigma} \in \mathbb{R}^{m\times n}$ is a diagonal matrix of singular values, and $\mathbf{V}^H \in \mathbb{C}^{n\times n}$ is a matrix of right singular vectors. Matrices $\mathbf{U}$, $\boldsymbol{\Sigma}$, and $\mathbf{V}$ are truncated such that close-to-zero singular values get discarted, resulting in matrices $\mathbf{U}_r \in \mathbb{C}^{m\times r}$, $\boldsymbol{\Sigma}_r \in \mathbb{R}^{r\times r}$, and $\mathbf{V}_r \in \mathbb{C}^{r\times m}$, where r is a number of singular values kept. Truncated matrices are used to calculate the Moore–Penrose inverse of the interface matrix: $\left(\mathbf{B}_c\mathbf{Y}\mathbf{B}_e^T\right)^+ = \mathbf{V}_r\boldsymbol{\Sigma}_r^{-1}\mathbf{U}_r^H$ [34].

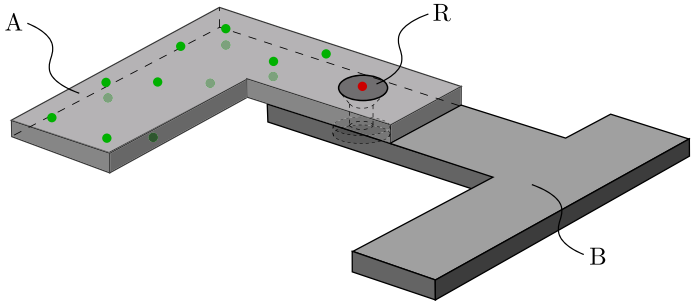

Fig. 2. System ARB with interface DoFs (●) and internal DoFs (●) of metal sheet plate A.

$$\mathbf{Y}^{\mathrm{R}} = \mathbf{L}_{\mathrm{c}}\widetilde{\mathbf{Y}}\mathbf{L}_{\mathrm{e}}, \tag{9}$$

where $\mathbf{L}_{\mathrm{c}}$ is a localization matrix extracting the rows of $\widetilde{\mathbf{Y}}$ corresponding to the riveted joint response DoFs, and $\mathbf{L}_{\mathrm{e}}$ is a localization matrix extracting the columns of $\widetilde{\mathbf{Y}}$ corresponding to the riveted joint excitation DoFs. Assuming the following sizes of matrices: $\mathbf{Y}^{\mathrm{A}} \in \mathbb{C}^{m_{\mathrm{A}}\times n_{\mathrm{A}}}$, $\mathbf{Y}^{\mathrm{B}} \in \mathbb{C}^{m_{\mathrm{B}}\times n_{\mathrm{B}}}$, $\mathbf{Y}^{\mathrm{R}} \in \mathbb{C}^{m_{\mathrm{R}}\times n_{\mathrm{R}}}$, and that both excitation and response DoFs in $\widetilde{\mathbf{Y}}$ belonging to assembly ARB are ordered as follows: internal DoFs of A, internal DoFs of B, interface DoFs of A, interface DoFs of B, localization matrices are structured as follows:

$$\mathbf{L}_{\mathrm{c}} = \begin{bmatrix}\mathbf{0}_{m_{\mathrm{R}}\times(m_{\mathrm{A}}+m_{\mathrm{B}}-m_{\mathrm{R}})} & \mathbf{I}_{m_{\mathrm{R}}\times m_{\mathrm{R}}} & \mathbf{0}_{m_{\mathrm{R}}\times m_{\mathrm{A}}} & \mathbf{0}_{m_{\mathrm{R}}\times m_{\mathrm{B}}}\end{bmatrix}, \tag{10}$$

and

$$\mathbf{L}_{\mathrm{e}} = \begin{bmatrix}\mathbf{0}_{n_{\mathrm{R}}\times(n_{\mathrm{A}}+n_{\mathrm{B}}-n_{\mathrm{R}})} & \mathbf{I}_{n_{\mathrm{R}}\times n_{\mathrm{R}}} & \mathbf{0}_{n_{\mathrm{R}}\times n_{\mathrm{A}}} & \mathbf{0}_{n_{\mathrm{R}}\times n_{\mathrm{B}}}\end{bmatrix}^{\mathrm{T}}. \tag{11}$$

2.3. Insight into the riveted-joint model

An important characteristic of the riveted-joint model $\mathbf{Y}^{\mathrm{R}}$ is that it depends not only on the material properties of the rivet, but also on the contact conditions at the interface (Fig. 3a). These contact conditions are influenced by the frictional properties between the metal sheet plates and between each plate and the rivet (e.g., material properties, surface roughness). As the stress distribution (Fig. 3b)[6] is strongly affected by the rivet-squeezing force [9], it is expected that there is a correlation between the dynamic properties of the joint and the rivet-squeezing force.

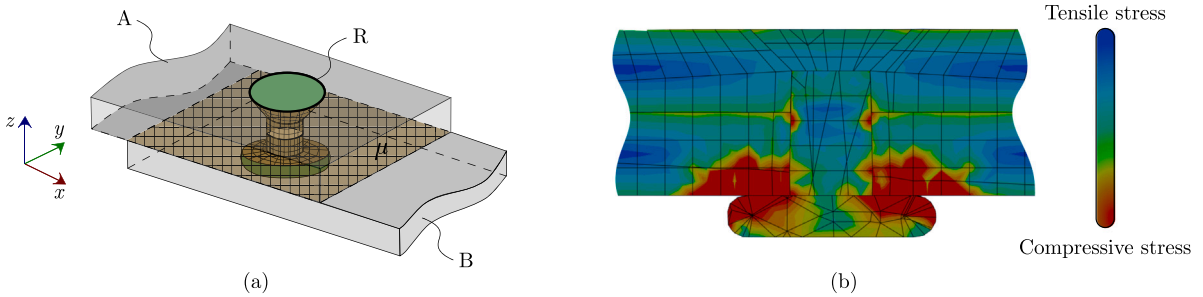

Fig. 3. Riveted-joint contact: (a) friction-affected surfaces (marked with grid) within the riveted joint, (b) stress distribution within the riveted joint.[7]

Frictional forces affect the joint's dynamic properties differently depending on the direction. For example, in the case of one rivet, it is expected that it significantly contributes to the stiffness around the z-axis, as it is the only force that prevents the relative motion of the metal sheet plates. So in order to efficiently characterize these effects in the squeezing-identification process, a sufficient set of DoFs has to be captured within the joint model (translational as well as rotational DoFs). The approach presented in Section 2.2 requires models $\mathbf{Y}^{\mathrm{ARB}}$, $\mathbf{Y}^{\mathrm{A}}$, and $\mathbf{Y}^{\mathrm{B}}$, which can be obtained either experimentally (measurement of FRFs) or numerically (e.g., Finite Element Analysis). However, due to its complexity, it can be difficult to realistically capture the joint's contact properties within the numerical experiment; therefore, the experimental approach is more commonly utilized. Within experimental approach we can

[6] Note that the residual stress field is significantly affected by the type of the riveting process, e.g. in the cold riveting process, residual stresses in rivet's axial direction can be assumed negligible, as the radial stresses can be as much as 10-times higher than axial (rivet extends in width) [36], hot riveting process results in residual stresses due to the thermal contraction of the rivet material after concluded riveting process, etc.

[7] See footnote 6.

obtain models with up to three observed response/excitation DoFs (translations in x, y, and z direction) per observed location (Fig. 4a). This means that the resulting joint models would enclose the same set of DoFs as the input models, containing no (direct) information about the rotational DoFs. For this reason, a Virtual Point Transformation (VPT) is performed on the DoFs corresponding to the nodes in the vicinity of the interface of models $\mathbf{Y}^{\mathrm{ARB}}$, $\mathbf{Y}^{\mathrm{A}}$, and $\mathbf{Y}^{\mathrm{B}}$. This allows us to project displacements/forces from multiple nodes, located close to the interface with three translational DoFs controlled/observed per node into a single node with six DoFs (3 translations and 3 rotations), called a Virtual Point (VP; Fig. 4a) [37,38]. The VPT is presented in more detail in the following.

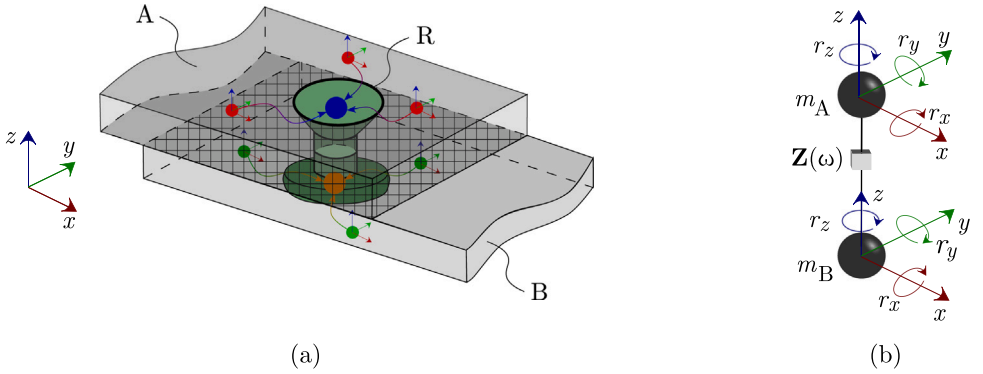

Fig. 4. Obtaining a joint model: (a) projection of responses/excitations from multiple 3 DoF nodes into the 6 DoF VP; (b) resulting model of the joint, consisting of 2 points of mass with 6 DoFs each. (●) Observed/controlled DoFs close to the interface on substructure A, (●) VP on substructure A, (●) observed/controlled DoFs close to the interface on substructure B, (●) VP on substructure B.

2.4. VPT

For the purpose of the VPT the displacements of the nodes in vicinity of the interface (stored in a vector of displacements $\boldsymbol{u} \in \mathbb{R}^a$, where a is a number of observed response DoFs) have to be related to the displacements of the VP (stored in a vector of displacements $\boldsymbol{q} \in \mathbb{R}^b; b \leq a$, where b is a number of VP response DoFs). Kinematic relations connecting $\boldsymbol{u}$ and $\boldsymbol{q}$ can be written in the form of Interface Deformation Mode (IDM) matrix $\mathbf{R}_{\mathrm{u}} \in \mathbb{R}^{a \times b}$[8] [39]:

$$\boldsymbol{u} = \mathbf{R}_{\mathrm{u}}\boldsymbol{q} + \boldsymbol{\mu}, \tag{12}$$

where $\boldsymbol{\mu}$ is a vector of residual displacements, which cannot be described by the IDM matrix $\mathbf{R}_{\mathrm{u}}$. In order to minimize the residuals $\boldsymbol{\mu}$, Eq. (12) is solved in a least-squares sense. Adding a constraint $\mathbf{R}_{\mathrm{u}}^{\mathrm{T}}\boldsymbol{\mu} = \mathbf{0}$, Eq. (12) can be solved for $\boldsymbol{q}$ as follows:

$$\boldsymbol{q} = \mathbf{T}_{\mathrm{u}}\boldsymbol{u}; \quad \mathbf{T}_{\mathrm{u}} = \left(\mathbf{R}_{\mathrm{u}}^{\mathrm{T}}\mathbf{R}_{\mathrm{u}}\right)^{-1}\mathbf{R}_{\mathrm{u}}^{\mathrm{T}}, \tag{13}$$

where $\mathbf{T}_{\mathrm{u}}$ is a displacement-transformation matrix. In a similar manner, excitation DoFs of nodes in the vicinity of interface can be projected into the VP excitation DoFs by using the force-transformation matrix, defined as [37]:

$$\mathbf{T}_{\mathrm{f}}^{\mathrm{T}} = \mathbf{R}_{\mathrm{f}}\left(\mathbf{R}_{\mathrm{f}}^{\mathrm{T}}\mathbf{R}_{\mathrm{f}}\right)^{-1}, \tag{14}$$

where $\mathbf{R}_{\mathrm{f}}$ is an IDM matrix containing relations between the excitation DoFs in the vicinity of the interface and the VP excitation DoFs. The transformation matrices $\mathbf{T}_{\mathrm{u}}$ and $\mathbf{T}_{\mathrm{f}}$ can be applied to transform the admittance matrix $\mathbf{Y}$ (containing DoFs in the vicinity of the interface) into the admittance matrix $\mathbf{Y}_{\mathrm{VPT}}$ (containing VP DoFs) [37]:

$$\mathbf{Y}_{\mathrm{VPT}} = \mathbf{T}_{\mathrm{u}}\mathbf{Y}\mathbf{T}_{\mathrm{f}}^{\mathrm{T}}. \tag{15}$$

By performing the VPT on the matrices $\mathbf{Y}^{\mathrm{A}}$, $\mathbf{Y}^{\mathrm{B}}$, and $\mathbf{Y}^{\mathrm{ARB}}$, we obtain the models $\mathbf{Y}^{\mathrm{A}}$ and $\mathbf{Y}^{\mathrm{B}}$, each containing a VP and selected set of internal DoFs (for extended interface decoupling), as well as model $\mathbf{Y}^{\mathrm{ARB}}$ with two VPs (one on the interface between substructure A and the rivet and the other one on the interface between the substructure B and the rivet) and a set of internal DoFs, corresponding to those selected on substructures A and B.

These models are used in the joint-characterization approach (Section 2.2) to obtain a model of the riveted joint. Such a model consists of two points of mass, treated as 6-DoF systems, thus 12-DoFs joint model (Fig. 4b). It should be noted that the resulting joint model does not only describe the dynamic properties of the rivet, but rather the dynamics of the contact between substructures A and B, which are affected by the properties of the rivet, as well as by the friction between each of the substructures and the rivet, and by the friction between the substructures themselves.

[8] IDM matrix $\mathbf{R}_{\mathrm{u}}$ contains a system of equations connecting the translations of each DoF in the vicinity of the interface to the chosen set of DoFs of the VP; these are usually translations and rotations (rigid IDMs), but extension, torsion, skewing, and bending modes (flexible IDMs) can also be included [39].

3. Procedure to the rivet-squeezing force estimation

In order to identify the rivet-squeezing force and assess the adequacy of the riveted joint, a non-destructive method is proposed that can be effectively used in EoL testing. The proposed approach for the rivet-squeezing force estimation is presented in Fig. 5. It generally relies on the LM FBS decoupling procedure to first obtain the joint admittances. In this process, the rivet admittance $\mathbf{Y}^{\mathrm{R}}(\omega)$ is inverted to acquire the mechanical impedance of the rivet $\mathbf{Z}_{\mathrm{J}}^{\mathrm{R}}(\omega)$.[9] This method allows for the creation of a reference joint dataset, in which the rivet-squeezing force corresponding to each joint admittance is deduced based on measurements. This dataset is then used to identify the riveting force for the structure of interest. As shown in Fig. 5, the assembly structure generally differs from the one from which the reference database was obtained; however, the metal sheets in contact should have similar thickness and material type to those used when constructing the joint dataset.

In the following, the rivet-squeezing force $\mathrm{F}_{\mathrm{s,u}}(\omega)$ for the joint of interest is estimated by evaluating the correlation between the joint's impedance $\mathbf{Z}_{\mathrm{u}}^{\mathrm{R}}(\omega)$ and the dataset joints' impedances $\mathbf{Z}_{\mathrm{J},i}^{\mathrm{R}}(\omega)$. $\mathrm{F}_{\mathrm{s,u}}(\omega)$ is then assigned a value $\mathrm{F}_{\mathrm{s,k}}(\omega)$ of a kth dataset sample for which the similarity between $\mathbf{Z}_{\mathrm{u}}^{\mathrm{R}}(\omega)$ and $\mathbf{Z}_{\mathrm{J,k}}^{\mathrm{R}}(\omega)$ is the highest (Fig. 5). In the following, details regarding the joint dataset as well as the estimation of the rivet-squeezing force will be presented.

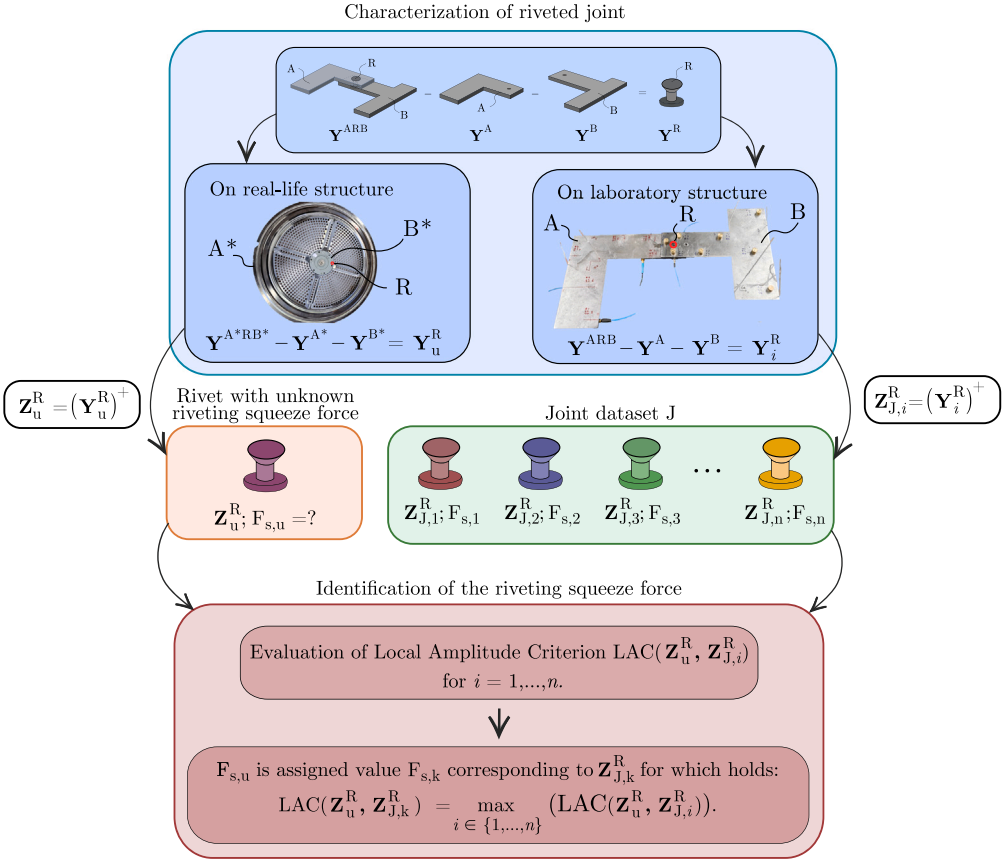

Fig. 5. Rivet characterization and rivet-squeezing-force identification flowchart.

3.1. Reference joint dataset J

The FBS-based approach, described in Section 2.2, is used to build a joint dataset containing impedance matrices $\mathbf{Z}_{\mathrm{J},i}^{\mathrm{R}}$ ($\mathbf{Z}_{\mathrm{J},i}^{\mathrm{R}} = \left(\mathbf{Y}_{i}^{\mathrm{R}}\right)^{+}$ for $i = 1, \ldots, r$) with known corresponding rivet-squeezing force $\mathrm{F}_{\mathrm{s},i}$ (measured during the riveting process).

Haeussler et al. [22], and Kreutz et al. [23] have shown that the dynamic model of the joint R, obtained by dynamic decoupling of the other system components, is independent of the properties of the original assembly. Thus, the joint obtained from the assembly ARB can be directly compared to the joint obtained from some modified assembly A'RB'. In the case of the riveted joint, this means that the joints from different assemblies riveted together by applying a similar squeezing force are expected to exhibit similar dynamic properties. Therefore, the reference dataset can be obtained from laboratory structures, while the joints for which we

[9] It is a common approach that the joint properties are analyzed on the impedance form of FRFs as it provides information on how a joint resists external loads, i.e. stiffness of the joint.

would like to identify the squeezing force are obtained from more complex, real-life assemblies. This assumption is valid as long as the joint's properties are similar in both assemblies in terms of the rivet material and geometry, and the frictional properties at the contact areas. Contact areas can vary in size, however, contact area should not be smaller than the area under compressive area affected caused by the riveted-joint [40], as this would cause differences in frictional forces in the contact between metal sheet plates and consequently differences in dynamic stiffness of the joint.

The size of the joint dataset and the distribution of the squeezing forces captured in the dataset, determine the degree of accuracy with which the squeezing force can be classified. The range of squeezing-force identification is limited to the squeezing forces applied to the joint that are measured in the joint dataset. This means that the accuracy of the identified force depends on the number of classes (measured force levels) in the reference joint dataset.[10]

3.2. Identification of the rivet-squeezing force

Having a reference joint dataset available, the squeezing force can be estimated in a manner of the Nearest Neighbor Search [41]. This means that we evaluate the resemblance between the impedance $\mathbf{Z}_{\mathrm{u}}^{\mathrm{R}} \in \mathbb{C}^{m\times n\times o}$ (where m is a number of observed response DoFs, n is a number of controlled excitation DoFs, and o is a number of discrete frequency points gathered in a set Ω) and the impedances of the dataset joints $\mathbf{Z}_{\mathrm{J},i}^{\mathrm{R}} \in \mathbb{C}^{m\times n\times o}$. For comparison of impedance $\mathbf{Z}_{\mathrm{u}}^{\mathrm{R}}$ to the impedance of the ith sample of the joint dataset $\mathbf{Z}_{\mathrm{J},i}^{\mathrm{R}}$, Local Amplitude Criterion (LAC) is proposed [42,43][11]:

$$\mathbf{LAC}^{\mathrm{u},i} = \mathrm{LAC}(\mathbf{Z}_{\mathrm{u}}^{\mathrm{R}},\ \mathbf{Z}_{\mathrm{J},i}^{\mathrm{R}}) = \frac{2\left|\mathbf{Z}_{\mathrm{u}}^{\mathrm{R}*} \odot \mathbf{Z}_{\mathrm{J},i}^{\mathrm{R}}\right|}{\left(\mathbf{Z}_{\mathrm{u}}^{\mathrm{R}*} \odot \mathbf{Z}_{\mathrm{u}}^{\mathrm{R}}\right) \odot \left(\mathbf{Z}_{\mathrm{J},i}^{\mathrm{R}*} \odot \mathbf{Z}_{\mathrm{J},i}^{\mathrm{R}}\right)}, \tag{16}$$

where * denotes the complex conjugate and $\mathbf{LAC}^{\mathrm{u},i} \in \mathbb{R}^{m\times n\times o}$ is a matrix of LAC values between each excitation and each response DoF at each discrete frequency point of matrices $\mathbf{Z}_{\mathrm{u}}^{\mathrm{R}}$ and $\mathbf{Z}_{\mathrm{J},i}^{\mathrm{R}}$.

Once the LAC values have been evaluated, for each of the r joint dataset samples, the sample, most similar to the joint of interest ($\mathbf{Z}_{\mathrm{u}}^{\mathrm{R}}$) has to be determined. Currently each matrix $\mathbf{LAC}^{\mathrm{u},i}$ consists of $m\times n\times o$ elements, which makes a direct comparison of individual LAC matrices difficult. For this reason, these can be represented by a single scalar value, e.g. by averaging all values within each LAC matrix. However, especially when dealing with experimental data, sufficient data quality can only be expected within a limited frequency range.[12] For this reason matrix $\mathbf{LAC}^{\mathrm{u},i}$ should be averaged in the frequency range of interest Ω' ($\Omega' \subseteq \Omega$):

$$\overline{\mathbf{LAC}}^{\mathrm{u},i} = \frac{1}{|\Omega'|} \sum_{\omega_l \in \Omega'} \mathbf{LAC}^{\mathrm{u},i}(\omega_l). \tag{17}$$

It is expected that the effects of variation in rivet-squeezing force will be most pronounced for a particular subset of excitation/response DoFs.[13] For this reason, the average can be calculated for P', a subset of the set P containing all elements of matrix $\overline{\mathbf{LAC}}^{\mathrm{u},i}$ (e.g. $P' = \{\overline{\mathbf{LAC}}_{1,1}^{\mathrm{u},i}, \overline{\mathbf{LAC}}_{2,3}^{\mathrm{u},i}, \overline{\mathbf{LAC}}_{4,6}^{\mathrm{u},i}, \dots\}$, where $\overline{\mathbf{LAC}}_{j,k}^{\mathrm{u},i}$ is an element located in the jth row and kth column of matrix $\overline{\mathbf{LAC}}^{\mathrm{u},i}$):

$$\overline{\mathrm{LAC}}^{\mathrm{u},i} = \frac{1}{|P'|} \sum_{p' \in P'} p'. \tag{18}$$

Finally, identification of the squeezing force narrows down to a simple classification problem in which $\mathrm{F}_{\mathrm{s,u}}$ is assigned a value $\mathrm{F}_{\mathrm{s,k}}$ of kth sample for which holds:

$$\overline{\mathrm{LAC}}^{\mathrm{u,k}} = \max_{j\in\{1,\dots,r\}} \overline{\mathrm{LAC}}^{\mathrm{u},j}. \tag{19}$$

4. Experimental validation

The proposed approach to the identification of the rivet-squeezing force was demonstrated and validated in a laboratory case study. Measurements were performed to build the models (i.e. admittance matrices) of structures, required to obtain joint models in a manner described in methodology of approach. Riveted joint models considering seven different squeezing forces were proposed to build a reference joint dataset. The approach was validated on the three samples obtained from a modified system.

[10] Maximum deviation of actual squeezing force from the identified value can be determined based on the differences between the joint dataset squeezing forces.

[11] Higher value of LAC criterion implies higher degree of similarity between FRFs.

[12] Experimental FRFs often deviate from the actual structure's response in the higher frequency range due to the insufficient excitation within that frequency range.

[13] In Section 2.3 it has been exposed that rivet-squeezing force strongly affects FRFs related to rotational DoFs around z-axis, i.e. rotations and moments around z-axis (Fig. 4).

4.1. Experimental setup

The laboratory structure of interest consists of two steel plates, A and B, riveted together to obtain the assembled systems ARB and A'RB' (Fig. 6). Here, the difference between the two assemblies is not in different substructures but in different interface conditions. Please note that the riveting location differs between the configurations ARB and A'RB'. Therefore, the dynamic properties of assemblies ARB and A'RB' differ from each other. The assembly ARB was used to obtain joint models for building a reference joint dataset, and the assembly A'RB' was used as a validation joint for which the squeezing riveting force is to be determined. All the assemblies were riveted using a hydraulic riveting system with a pressure sensor to obtain accurate reference squeezing forces.

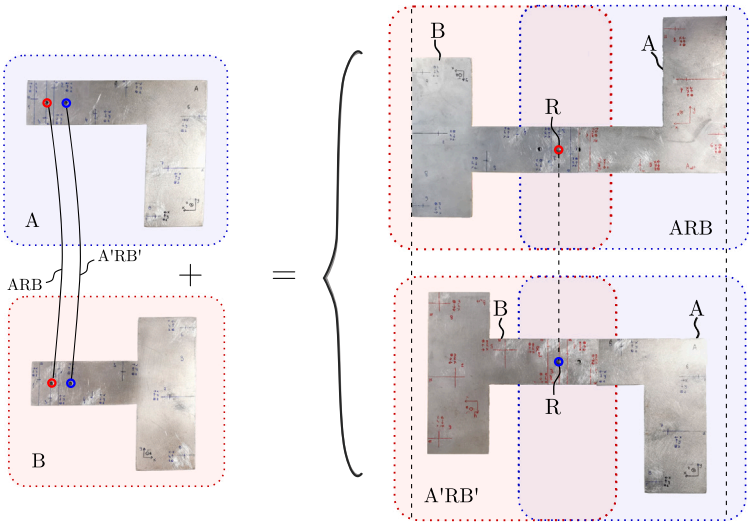

Fig. 6. Laboratory structures: steel plates A and B, and assemblies ARB and A'RB'.

The first step towards the joint rivet-squeezing force identification is to obtain joint dynamics properties in the form of their corresponding mechanical impedances $\mathbf{Z}_{\mathrm{J}}^{\mathrm{R}}$. Each of these is a result of a dynamic decoupling process using FBS methods, thoroughly described in Section 2. The following inputs are required for dynamic decoupling: the admittance matrix of the assembled system $\mathbf{Y}^{\mathrm{ARB}}$, the admittance matrices of substructures A and B ($\mathbf{Y}^{\mathrm{A}}$ and $\mathbf{Y}^{\mathrm{B}}$, respectively), and the Boolean matrices $\mathbf{B}_{\mathrm{c}}$ and $\mathbf{B}_{\mathrm{e}}$. The admittance matrices $\mathbf{Y}^{\mathrm{ARB}}$, $\mathbf{Y}^{\mathrm{A}}$, and $\mathbf{Y}^{\mathrm{B}}$ were obtained experimentally. For the extended interface decoupling technique, FRFs in internal as well as DoFs in the vicinity of the interface (for the purpose of VPT) of each structure were measured. Internal DoFs were observed/controlled at five measurement locations per substructure, dispersed over the entire structure, while the DoFs intended for the VPT were observed/controlled at three measurement locations per substructure. The responses to the excitation force at these locations were observed using three-axial accelerometers (Dytran 3273A2, PCB 356A45, and PCB TLD356A32). Due to the large number of response points in the measurement of the assembled system ARB, measurements had to be performed in two steps, moving the accelerometers between measurement points, according to the roving-sensor approach. To prevent changes in the system dynamics due to variations in the mass distribution between each step, brass masses were attached to the points where the sensor was missing in each step of the measurement campaign. At each location, an excitation force was applied in three directions, using a modal hammer PCB 086C03 (Fig. 7). Excitation forces were applied directly on accelerometers/brass masses with amplitudes no higher than 24 N to avoid nonlinearities. During the measurements, the structures were suspended from elastic strings, simulating free boundary conditions (Fig. 7).

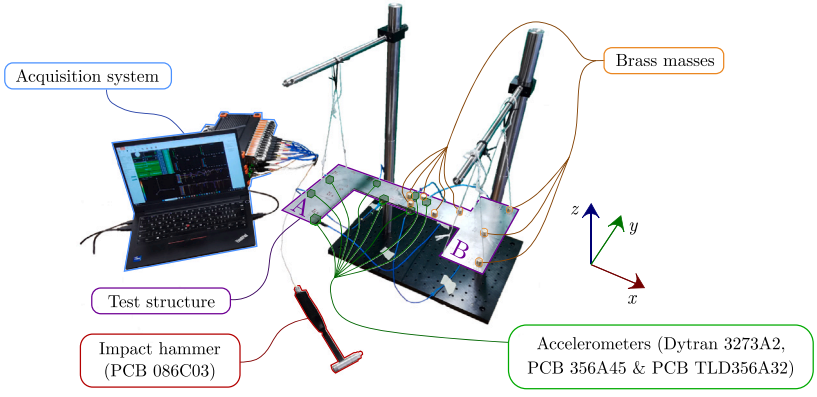

Fig. 7. Experimental setup.

4.2. Building the reference joint dataset

The force and acceleration signals, resulting from the impact testing, were used to estimate the FRFs between each pair of the controlled/observed DoFs and in this way obtaining the admittance matrices, $\mathbf{Y}^{\mathrm{A}} \in \mathbb{C}^{24\times24}$, $\mathbf{Y}^{\mathrm{B}} \in \mathbb{C}^{24\times24}$ and $\mathbf{Y}^{\mathrm{ARB}} \in \mathbb{C}^{48\times48}$. Applying the VPT to these admittance matrices (Eq. (15)), DoFs in vicinity of the interface were transformed into one 6-DoF VP for each of the substructures A and B and into two 6-DoF VPs for the assembled system ARB (VP corresponding to DoFs at component A, and VP corresponding to DoFs at component B). Thus, the matrices $\mathbf{Y}^{\mathrm{A}}$, $\mathbf{Y}^{\mathrm{B}}$ and $\mathbf{Y}^{\mathrm{ARB}}$ were reduced into $\mathbf{Y}^{\mathrm{A}} \in \mathbb{C}^{21\times21}$, $\mathbf{Y}^{\mathrm{B}} \in \mathbb{C}^{21\times21}$ and $\mathbf{Y}^{\mathrm{ARB}}_{\mathrm{VPT}} \in \mathbb{C}^{42\times42}$, respectively.

To build the reference joint dataset the measurements had to be performed on multiple assembled systems ARB riveted with different squeezing forces. Seven assemblies riveted with different squeezing forces were constructed, resulting in the admittance matrices $\mathbf{Y}^{\mathrm{ARB}}_{\mathrm{VPT},i}$ where $i \in F_{\mathrm{s,J}}$ ($F_{\mathrm{s,J}}$ denotes a set of squeezing forces captured within the reference dataset; $F_{\mathrm{s,J}}$ = {5.0 kN, 8.3 kN, 9.2 kN, 10.0 kN, 10.8 kN, 11.7 kN, 15.0 kN}).

The measurements on substructures A and B were performed to obtain the substructure admittances $\mathbf{Y}^{\mathrm{A}}_{\mathrm{VPT}}$ and $\mathbf{Y}^{\mathrm{B}}_{\mathrm{VPT}}$. These are then decoupled from assembled system admittances $\mathbf{Y}^{\mathrm{ARB}}_{\mathrm{VPT},i}$, as described in Section 2, resulting in joint admittances $\mathbf{Y}^{\mathrm{R}}_{i}$. During the process, interface matrix $\mathbf{B}_{\mathrm{c}}\mathbf{Y}\mathbf{B}^{\mathrm{T}}_{\mathrm{e}}$ in the LM FBS Eq. (7) has been identified as ill-conditioned. Fig. 8a displays singular values of the interface matrix for the sample riveted together by applying 15.0 kN squeezing force. It can be observed that there are only a few dominant singular values, while the vast majority of singular values are much smaller. Ill-conditioning of the interface matrix was also qualitatively evaluated by calculating the corresponding condition number (Fig. 8b).[14] High values of condition number at all frequencies additionally confirmed the ill-conditioned interface matrix. Due to this, TSVD has been performed in combination with the Moore–Penrose inverse (as described in Section 2.1) to obtain the inverse of the interface matrix needed in the LM FBS Eq. (7). Singular values lower than 10^{-3} times the maximum singular value at a given frequency were discarded, thus keeping only a few dominant singular values.

By inverting the joint admittances, a set of impedances $\{\mathbf{Z}^{\mathrm{R}}_{\mathrm{J},i} \mid i \in F_{\mathrm{s,J}}\}$ corresponding to given riveting squeezing force were obtained ($\mathbf{Z}^{\mathrm{R}}_{\mathrm{J},i} = \left(\mathbf{Y}^{\mathrm{R}}_{i}\right)^{+}$),[15] which (together with corresponding squeezing forces) compose the joint dataset J.

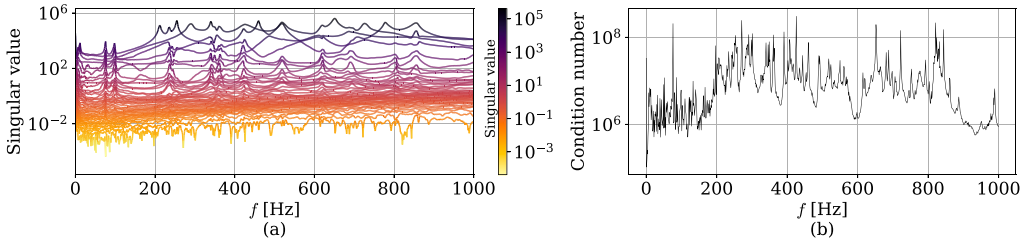

Fig. 8. SVD of the interface matrix $\mathbf{B}_{\mathrm{c}}\mathbf{Y}\mathbf{B}^{\mathrm{T}}_{\mathrm{e}}$ for sample with corresponding F_{s} = 15 kN: (a) singular values vs frequency, and (b) condition number.

4.3. Analysis of the effect of the rivet-squeezing force on the dynamic response of the structure

Before focusing on the identification of the rivet-squeezing force, it is necessary to investigate how the squeezing force actually affects the dynamic response of the system/assembly. Sample FRFs from the admittance matrices $\mathbf{Y}_{\mathrm{ARB},i}$ (connecting the same pair of excitation and response DoFs) with different squeezing forces are displayed in Fig. 9. By examining the resonance peaks of the FRFs, it can be observed that location and amplitude of specific resonance peaks depend strongly on the squeezing force $\mathrm{F_s}$. These peaks are singled out and presented individually in Fig. 9. Some peaks are altered in terms of amplitude (Figs. 9a and 9b), while for some other vibration modes, the corresponding natural frequency is also shifted (Figs. 9c and 9d).

Variations in the rivet-squeezing force hence cause distinct differences in the assembly dynamics. In our approach, the squeezing force identification relies on joint admittance identification $\mathbf{Y}^{\mathrm{R}}_{i}$ based on the FBS decoupling approach. By inverting the obtained joint admittances, this results in the dynamic stiffness matrices of the riveted joint $\mathbf{Z}^{\mathrm{R}}_{\mathrm{J},i}$. In order to find the elements of the dynamic stiffness matrix that hold information, valuable for the squeezing force identification, each FRF of each $\mathbf{Z}^{\mathrm{R}}_{\mathrm{J},i}$ has been divided into segments the size of 100 Hz for frequency range up to 1000 Hz (to investigate whether the effects of the squeezing force on the dynamic stiffness in some frequency ranges are more apparent than in others). For each segment an average dynamic stiffness was calculated. Vector of average segment dynamic stiffnesses $\bar{z}^{\Omega_r}_{\mathrm{J};m,n}$ for element in mth row and nth column of matrices $\mathbf{Z}^{\mathrm{R}}_{\mathrm{J},i}$ (i.e. $\mathbf{Z}^{\mathrm{R}}_{\mathrm{J},i;m,n}$ for $i \in F_{\mathrm{s,J}}$) within limited frequency range Ω_r ($\Omega_r \subseteq \Omega$) can be written as:

$$\bar{z}^{\Omega_r}_{\mathrm{J};m,n} = \left[\frac{1}{|\Omega_r|}\sum_{\omega_r\in\Omega_r}\left|\mathbf{Z}^{\mathrm{R}}_{\mathrm{J},i;m,n}(\omega_r)\right|\right]_{i\in F_{\mathrm{s,J}}} \tag{20}$$

[14] Condition number is defined as a ratio between the largest and the smallest singular value [44].

[15] Admittances are twice-integrated (which means double division by $i\omega$ for data in frequency domain) to convert accelerations to displacements. This way, the dynamic stiffness of the joint is obtained after admittance matrix inversion.

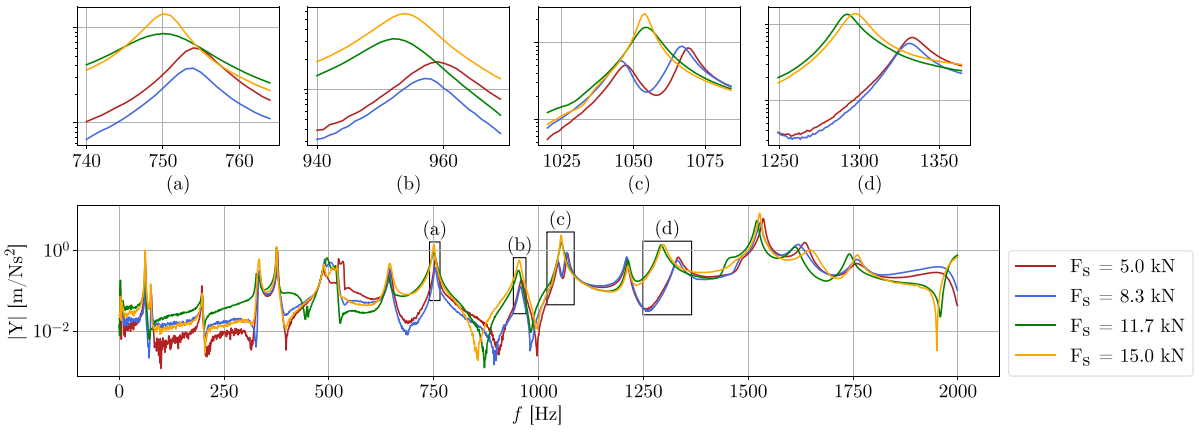

Fig. 9. Dynamic response of the assembly (excitation close to the interface at substructure B in y-direction and response close to the interface at substructure A in x-direction) for different rivet-squeezing forces F_s.

Resulting values were used to determine correlations between squeezing force and average dynamic stiffness of each element of $\mathbf{Z}_J^R$ within each frequency range. For element of mth row and nth column of $\mathbf{Z}_{J,i}^R$ (for $i \in F_{s,J}$) within frequency range Ω_r correlation $\rho_{m,n}^{\Omega_r}$ can be calculated by (to enhance readability, let $\boldsymbol{u} = \overline{\boldsymbol{z}}_{J;m,n}^{\Omega_r}$ and $\boldsymbol{v} = \mathrm{vec}(F_{s,J})$, each having $n_{u,v}$ elements):

$$\rho_{m,n}^{\Omega_r} = \frac{\sum_{i=1}^{n_{u,v}}(u_i - \overline{u})(v_i - \overline{v})}{\sqrt{\sum_{i=1}^{n_{u,v}}(u_i - \overline{u})^2}\sqrt{\sum_{i=1}^{n_{u,v}}(v_i - \overline{v})^2}}. \tag{21}$$

To identify elements of $\mathbf{Z}_J^R$ that exhibit overall high potential for identification of squeezing force, average value of absolute values.[16] of correlations were calculated for each element. Results for bottom left part of $\mathbf{Z}_J^R$ (i.e. excitations at point of mass m_A and corresponding responses at point of mass m_B) are displayed in Fig. 10 From the chart it can be observed that the dynamic stiffness between rotation r_z of m_B and force F_x at m_A exhibits by far the highest correlation (i.e. 0.813). There are some other components with relatively high correlation, e.g. component with excitation M_z at m_A and response r_z at m_B (average correlation of 0.705), and component with excitation M_z at m_A and response in the x-direction at m_B (average correlation of 0.656). However as these correlations are considerably lower, the dynamic stiffness between rotation r_z of m_B and force F_x at m_A was recognized as the most promising element of $\mathbf{Z}_J^R$ for identification of the squeezing force for validation samples.

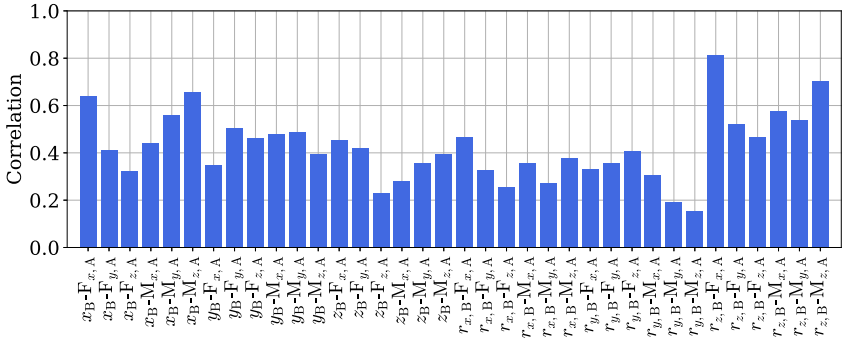

Fig. 10. Average of absolute correlations over all segments for elements of the dynamic stiffness matrix with excitations at point of mass m_B and responses at point of mass m_A.

Sample dynamic stiffness graphs connecting rotation r_z of joint's point mass m_B to the force F_x corresponding to the point of mass m_A (Fig. 4b) are displayed in Fig. 11. Within a lower frequency range (up to approx. 50 Hz), dynamic stiffness is affected by imperfections in the experimental approximation of the free boundary conditions. In addition to that, it is possible to observe that the differences between the dynamic stiffnesses corresponding to 5.0 kN and 8.3 kN samples as well as the differences between the 11.7 kN and 15.0 kN sample become substantially less distinct in the higher frequency range, making it difficult to distinguish between the various squeezing forces. This could lead to a reduced accuracy of the rivet-squeezing force estimation in the following.

[16] Absolute value has been used to account for highly negative correlations which can still provide meaningful information for identification of squeezing force.

Therefore, we are focusing on the frequency range between 50 Hz and 300 Hz, which was identified as appropriate for efficient squeezing-force identification for given structure.

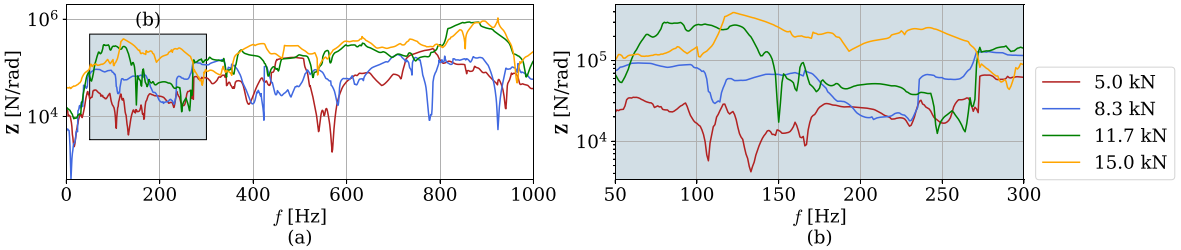

Fig. 11. Dynamic response of the joint (connecting rotation r_z of joint's point mass m_B to the force F_x corresponding to the point of mass m_A) for different rivet-squeezing forces F_s: (a) freq. range between 0 Hz and 1000 Hz, and (b) freq. range between 50 Hz and 300 Hz.

4.4. Identification of the rivet-squeezing force

To validate the proposed approach, the squeezing force identification was performed on the modified assembly A'RB'. It has been demonstrated in [29], that after the decoupling procedure, some residual dynamics of the assembly can remain in the resulting dynamic response (commonly in form of spurious peaks). This is due to measurement errors or/and unobserved and uncontrolled assembly dynamics. It can be observed in Fig. 12 that the resonance peaks of the assemblies ARB and A'RB' are located in considerably different locations. Due to this, the residual dynamics in the joint model, obtained by dynamic decoupling, differs for the joints obtained from assembly ARB compared to the one obtained from A'RB', despite keeping the same set ob substructures A and B. Due to this, it can be reasonably assumed that the joint models are valid for other assemblies with similar joint properties. This is additionally supported by the article written by Haeussler et al. [22] and the article written by Kreutz et al. [23] which tested the transferability of the joints obtained using FBS.

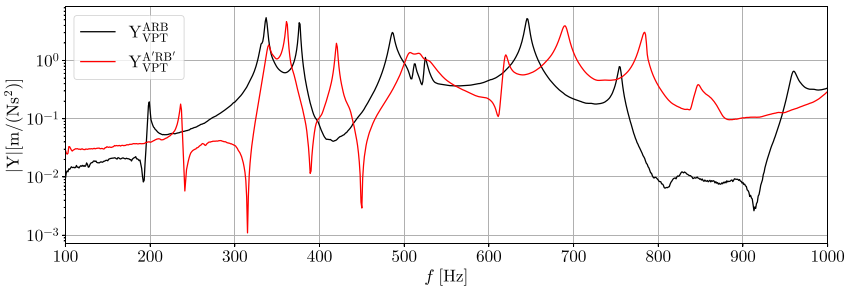

Fig. 12. FRFs of the assembled systems ARB and A'RB'; connecting excitations F_z at VP at structure B/B' to responses u_x at VP at structure A/A'.

To assess the accuracy of the proposed approach, three validation samples were obtained with different squeezing forces. To determine the reference squeezing forces, the validation samples were riveted together in a highly monitored environment with the force being measured during the riveting process. The process of obtaining riveted joint models from validation assemblies matches the one for obtaining the reference dataset joints. Measurements of the dynamic responses were performed on assembled systems A'RB'. Because the location of the riveted joint changes (compared to assembly ARB), sensor and impact locations had to be changed. For this reason, the admittances of each substructure also had to be performed anew. Substructures A and B were then decoupled from the assembly A'RB' (using TSVD and Moore–Penrose inverse to deal with ill-conditioned interface matrix in Eq. (7)), resulting in joint impedances $\mathbf{Z}^{R}_{v,8.3kN}$, $\mathbf{Z}^{R}_{v,10.8kN}$ and $\mathbf{Z}^{R}_{v,15kN}$, with reference squeezing forces of 8.3 kN, 10.8 kN and 15.0 kN, respectively.

In the following, the squeezing forces $F_{s,v}$, corresponding to the validation samples, were identified based on the reference dataset by evaluating LAC criterion between the validation sample $\mathbf{Z}^{R}_{v}$ and each dataset sample $\mathbf{Z}^{R}_{J}$. The $\mathrm{LAC}\left(\mathbf{Z}^{R}_{v,i}, \mathbf{Z}^{R}_{J,j}\right)$ criterion was evaluated using Eq. (16) for $i \in \{8.3\text{ kN}, 10.8\text{ kN}, 15.0\text{ kN}\}$, $j \in \{5.0\text{ kN}, 8.3\text{ kN}, 9.2\text{ kN}, 10.0\text{ kN}, 10.8\text{ kN}, 11.7\text{ kN}, 15.0\text{ kN}\}$. The average value of LAC criterion was calculated in the frequency range between 50 Hz and 300 Hz.

In the process of rivet-squeezing force identification, dynamic stiffness that connects excitations in the x-direction at the joint's point of mass corresponding to component A to the rotations around the z-axis at the joint's point of mass corresponding to component B was used. The resulting averaged LAC values are presented in Fig. 13. Each value represents a single averaged LAC matrix between the validation sample (denoted by the corresponding reference squeezing force $F_{s,V}$) and the reference dataset sample (denoted by corresponding squeezing force $F_{s,J}$). The highest values of averaged LAC criterion indicates the best agreement between the joint impedance's and enable to identify the squeezing force of validation sample based on the reference dataset samples.

The results of the identification process demonstrates that for all three validation samples the riveting squeezing forces were correctly identified, i.e. the predicted riveting squeeze force matched the reference force obtained by direct measurements during riveting. Two out of three predictions (i.e., validation samples with 10.8 kN and 15.0 kN squeezing forces) can be accepted with a high degree of confidence. For the validation sample with a squeezing force of 8.3 kN, the deviation from the other dataset samples was less distinct. Nevertheless, the method correctly predicted the correct value of the riveting squeezing force. This validation

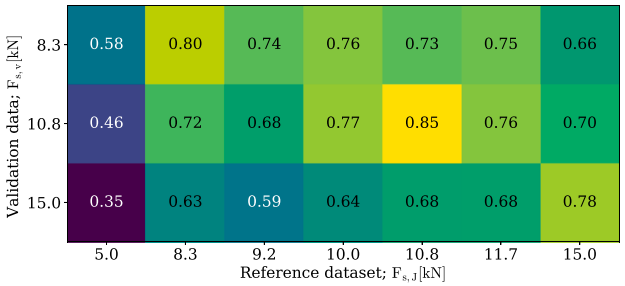

Fig. 13. Heat map displaying LAC value, evaluating the similarity between the FRF connecting the joint's rotation r_z with the excitation F_x of the validation samples $\mathbf{Z}_v^R$ (with corresponding reference squeezing forces $F_{s,v}$) and of reference joint dataset samples $\mathbf{Z}_{J,i}^R$ (with corresponding squeezing forces $F_{s,J}$).

example showcases that the proposed approach can be effectively used to identify the riveting squeezing force, even in the modified assembly.

5. Conclusions

In this paper, an approach to indirect riveting squeezing force identification is proposed. The FBS methodology is applied to isolate the dynamic model of the joint from the dynamic model of the assembled system. A significant advantage of this approach is that the joint of interest can originate from a modified structure or an entirely different assembly compared to the structure used to build the reference joint dataset. On the other hand, the approach is limited by requirement that the properties of the joint of interest are similar to those of dataset joints i.e. different geometry or material of the rivet requires a new reference joint dataset. Besides, the frictional properties of the components being riveted together have to be similar in vicinity of the riveted joint. Due to this, the proposed approach is especially convenient for manufacturing processes and condition monitoring for products where rivets of the same size and geometry are used to join metal sheet plates made of similar materials and undergone similar surface preparation.

The approach was tested on a real-life experimental setup. A small reference joint dataset, consisting of seven joint models with different corresponding squeezing forces, was built. Three validation samples were used for the squeezing force identification. Validation models were obtained from a modified version of the assembly used to build the joint dataset. Despite some deviations in certain force ranges, the method successfully predicted the rivet-squeezing forces for all validation samples, demonstrating its robustness and applicability in real-life scenarios. This methodology not only enhances the identification of rivet squeezing force but also provides a reliable, non-destructive testing approach for ensuring the quality and integrity of riveted joints in manufacturing processes.

Nevertheless, there still exists space for further research. In the real-life applications, commonly, multiple rivets are applied to fasten metal sheet plates together. The applicability of the proposed approach to such scenarios presents an interesting matter for further research.

CRediT authorship contribution statement

Tim Vrtač: Writing – original draft, Methodology, Investigation, Formal analysis, Conceptualization. **Miha Kodrič:** Writing – original draft, Validation, Methodology, Conceptualization. **Miha Pogačar:** Writing – original draft, Visualization, Validation. **Gregor Čepon:** Validation, Supervision, Methodology, Conceptualization.

Declaration of competing interest

The authors declare that they have no known competing financial interests or personal relationships that could have appeared to influence the work reported in this paper.

Acknowledgments

The authors acknowledge financial support from the European Union's Horizon Europe research and innovation programme under the grant agreement No. 101091536 (DiCiM project).

Data availability

No data was used for the research described in the article.

References

[1] J. Wu, C. Chen, Y. Ouyang, D. Qin, H. Li, Recent development of the novel riveting processes, Int. J. Adv. Manuf. Technol. 117 (2021) 19–47, http://dx.doi.org/10.1007/s00170-021-07689-w.

[2] M. Wall, M.S. Allen, R.J. Kuether, Observations of modal coupling due to bolted joints in an experimental benchmark structure, Mech. Syst. Signal Process. 162 (2022) 107968, http://dx.doi.org/10.1016/j.ymssp.2021.107968.

[3] Q. Li, Z. Li, M. Liao, F. Yang, X. Jing, Transmissibility function-based diagnosis of a class of bolted Beam-like structures with nonlinear fault-induced loads and nonlinear boundary conditions, Mech. Syst. Signal Process. 191 (2023) 110189, http://dx.doi.org/10.1016/j.ymssp.2023.110189.

[4] K. Mori, Y. Abe, T. Kato, Mechanism of superiority of fatigue strength for aluminium alloy sheets joined by mechanical clinching and self-pierce riveting, J. Mater. Process. Technol. 212 (9) (2012) 1900–1905, http://dx.doi.org/10.1016/j.jmatprotec.2012.04.017.

[5] J. Meggitt, Interval-based identification of response-critical joints in complex built-up structures: A tool for model refinement, J. Sound Vib. (2022) http://dx.doi.org/10.1016/j.jsv.2022.116850.

[6] S. Wang, J. Zhang, Z. Liu, X. Zhang, J. Hong, K. Nan, W. Wang, Riveting parameter design that satisfies requirements for driven rivet head dimensions, Proc. Inst. Mech. Eng. Part C: J. Mech. Eng. Sci. 229 (13) (2015) 2412–2432.

[7] M. Li, W. Tian, J. Hu, C. Wang, Z. Shi, W. Liao, Influence of riveting die configuration and squeeze force on the mechanical properties and fatigue behavior of aircraft lap joints, Eng. Fail. Anal. 142 (2022) 106772, http://dx.doi.org/10.1016/j.engfailanal.2022.106772.

[8] H. Zhang, Influence of riveting sequence/direction on distortion of steel and aluminum sheets, J. Manuf. Process. 53 (2020) 304–309, http://dx.doi.org/10.1016/j.jmapro.2020.02.039.

[9] R.P.G. Müller, An experimental and analytical investigation on the fatigue behaviour of fuselage riveted lap joints (Ph.D. thesis), TU Delft, 1995.

[10] M. Li, W. Tian, J. Hu, C. Wang, W. Liao, Effect of hole perpendicularity error and squeeze force on the mechanical behaviors of riveted joints, Microsc. Res. Tech. 85 (3) (2022) 1075–1088, http://dx.doi.org/10.1002/jemt.23977.

[11] C. Zeng, J.T. Xue, X.Y. Liu, W. Tian, Design variables influencing the fatigue of al 2024-T3 in riveted aircraft lap joints: Squeeze force and initial fit tolerance, Int. J. Fatigue 140 (2020) 105751, http://dx.doi.org/10.1016/j.ijfatigue.2020.105751.

[12] H. Huan, M. Liu, Effects of squeeze force on static behavior of riveted lap joints, Adv. Mech. Eng. 9 (5) (2017) http://dx.doi.org/10.1177/1687814016686891.

[13] C. Roberts, L.D. Avendaño-Valencia, D. García Cava, Robust mitigation of EOVs using multivariate nonlinear regression within a vibration-based SHM methodology, Mech. Syst. Signal Process. 208 (2024) 111028, http://dx.doi.org/10.1016/j.ymssp.2023.111028.

[14] A. Kamariotis, E. Chatzi, D. Straub, A framework for quantifying the value of vibration-based structural health monitoring, Mech. Syst. Signal Process. 184 (2023) 109708, http://dx.doi.org/10.1016/j.ymssp.2022.109708.

[15] A. Kamariotis, E. Chatzi, D. Straub, Value of information from vibration-based structural health monitoring extracted via Bayesian model updating, Mech. Syst. Signal Process. 166 (2022) 108465, http://dx.doi.org/10.1016/j.ymssp.2021.108465.

[16] J. Meggitt, R. McGee, On the limitations of transmissibility functions for damage localisation: the influence of completeness, Struct. Heal. Monit. (2024) http://dx.doi.org/10.1177/14759217241226602.

[17] J. Mucha, W. Witkowski, Mechanical behavior and failure of riveting joints in tensile and shear tests, Strength Mater. 47 (2015) 755–769, http://dx.doi.org/10.1007/s11223-015-9712-5.

[18] J. Maljaars, D. Leonetti, C. Maas, Fatigue life prediction of hot riveted double covered butt joints, Int. J. Fatigue 124 (2019) 99–112, http://dx.doi.org/10.1016/j.ijfatigue.2019.03.002.

[19] S. Mariani, Q. Rendu, M. Urbani, C. Sbarufatti, Causal dilated convolutional neural networks for automatic inspection of ultrasonic signals in non-destructive evaluation and structural health monitoring, Mech. Syst. Signal Process. 157 (2021) 107748, http://dx.doi.org/10.1016/j.ymssp.2021.107748.

[20] C. Gao, Z. Fang, J. Lin, X. Guan, J. He, Model averaging and probability of detection estimation under hierarchical uncertainties for Lamb wave detection, Mech. Syst. Signal Process. 165 (2022) 108302, http://dx.doi.org/10.1016/j.ymssp.2021.108302.

[21] A. Gay, J.-M. Roche, P. Lapeyronnie, F. Valiorgue, P. Bertrand, Non-destructive inspection of initial defects of PA6.6-GF50/aluminum self-piercing riveted joints and damage monitoring under mechanical static loading, Int. J. Damage Mech. 26 (8) (2017) 1127–1146, http://dx.doi.org/10.1177/1056789516648370.

[22] M. Haeussler, S. Klaassen, D. Rixen, Experimental twelve degree of freedom rubber isolator models for use in substructuring assemblies, J. Sound Vib. 474 (2020) 115253, http://dx.doi.org/10.1016/j.jsv.2020.115253.

[23] M. Kreutz, F. Trainotti, V. Gimpl, D. Rixen, On the robust experimental multi-degree-of-freedom identification of bolted joints using frequency-based substructuring, Mech. Syst. Signal Process. (2023) http://dx.doi.org/10.1016/j.ymssp.2023.110626.

[24] D. de Klerk, D.J. Rixen, S.N. Voormeeren, General framework for dynamic substructuring: History, review and classification of techniques, AIAA J. 46 (5) (2008) 1169–1181, http://dx.doi.org/10.2514/1.33274.

[25] D. de Klerk, D.J. Rixen, J. de Jong, The frequency based substructuring (FBS) method reformulated according to the dual domain decomposition method, in: Proceedings of the 24th International Modal Analysis Conference, a Conference on Structural Dynamics, 2006, pp. 1–14.

[26] M. van der Seijs, Experimental dynamic substructuring: Analysis and design strategies for vehicle development (Ph.D. thesis), Delft University of Technology, 2016, http://dx.doi.org/10.4233/uuid:28b31294-8d53-49eb-b108-284b63edf670.

[27] S. Voormeeren, D. Rixen, A family of substructure decoupling techniques based on a dual assembly approach, Mech. Syst. Signal Process. 27 (2012) 379–396, http://dx.doi.org/10.1016/j.ymssp.2011.07.028.

[28] D.J. Rixen, How measurement inaccuracies induce spurious peaks in frequency based substructuring, in: Proceedings of the Twenty Sixth International Modal Analysis Conference, Orlando, FL. Society for Experimental Mechanics, Bethel, CT, 2008.

[29] S.W. Klaassen, M.V. van der Seijs, D. de Klerk, System equivalent model mixing, Mech. Syst. Signal Process. 105 (2018) 90–112, http://dx.doi.org/10.1016/j.ymssp.2017.12.003.

[30] T.G. Carne, D. Griffith, M.E. Casias, Support conditions for free boundary-condition modal testing, Tech. rep., Sandia National Lab.(SNL-NM), Albuquerque, NM (United States), 2006.

[31] W. D'Ambrogio, A. Fregolent, Decoupling procedures in the general framework of frequency based substructuring, in: Proceedings of 27th IMAC. Orlando (USA), vol. 70, 2009.

[32] T. Lim, J. Li, A theoretical and computational study of the FRF-based substructuring technique applying enhanced least square and TSVD approaches, J. Sound Vib. 231 (4) (2000) 1135–1157, http://dx.doi.org/10.1006/jsvi.1999.2724.

[33] W. D'Ambrogio, A. Fregolent, The role of interface DoFs in decoupling of substructures based on the dual domain decomposition, Mech. Syst. Signal Process. 24 (7) (2010) 2035–2048, http://dx.doi.org/10.1016/j.ymssp.2010.05.007, Special Issue: ISMA 2010.

[34] T. Gialamas, D. Tsahalis, D. Otte, H. Van der Auwaraer, D. Manolas, Substructuring technique: improvement by means of singular value decomposition (SVD), Appl. Acoust. 62 (10) (2001) 1211–1219, http://dx.doi.org/10.1016/S0003-682X(00)00095-5.

[35] P.C. Hansen, Truncated singular value decomposition solutions to discrete ill-posed problems with ill-determined numerical rank, SIAM J. Sci. Stat. Comput. 11 (3) (1990) 503–518, http://dx.doi.org/10.1137/0911028.

[36] V. Blanchot, A. Daidie, Riveted assembly modelling: Study and numerical characterisation of a riveting process, J. Mater. Process. Technol. 180 (1) (2006) 201–209, http://dx.doi.org/10.1016/j.jmatprotec.2006.06.005.

[37] M.V. Van Der Seijs, D.D. van den Bosch, D.J. Rixen, D. de Klerk, An improved methodology for the virtual point transformation of measured frequency response functions in dynamic substructuring, in: 4th ECCOMAS Thematic Conference on Computational Methods in Structural Dynamics and Earthquake Engineering, vol. 4, 2013, http://dx.doi.org/10.7712/120113.4816.C1539.

[38] Z. Saeed, S.W.B. Klaassen, C.M. Firrone, T.M. Berruti, D.J. Rixen, Experimental joint identification using system equivalent model mixing in a bladed disk, J. Vib. Acoust. 142 (5) (2020) 051001, http://dx.doi.org/10.1115/1.4047361.

[39] E.A. Pasma, M.V.v.d. Seijs, S.W.B. Klaassen, M.W.v.d. Kooij, Frequency based substructuring with the virtual point transformation, flexible interface modes and a transmission simulator, in: A. Linderholt, M.S. Allen, R.L. Mayes, D. Rixen (Eds.), Dynamics of Coupled Structures, vol. 4, Springer International Publishing, 2018, pp. 205–213.

[40] M. Skorupa, T. Machniewicz, A. Skorupa, A. Korbel, Effect of load transfer by friction on the fatigue behaviour of riveted lap joints, Int. J. Fatigue 90 (2016) 1–11, http://dx.doi.org/10.1016/j.ijfatigue.2016.04.005.

[41] H.N. Mohammad Reza Abbasifard, A survey on nearest neighbor search methods, Int. J. Comput. Appl. 95 (25) (2014) 39–52, http://dx.doi.org/10.5120/16754-7073.

[42] C. Zang, H. Grafe, M. Imregun, Frequency–domain criteria for correlating and updating dynamic finite element models, Mech. Syst. Signal Process. 15 (1) (2001) 139–155, http://dx.doi.org/10.1006/mssp.2000.1357.

[43] D. Lee, T.-S. Ahn, H.-S. Kim, A metric on the similarity between two frequency response functions, J. Sound Vib. 436 (2018) 32–45, http://dx.doi.org/10.1016/j.jsv.2018.08.051.

[44] N. Maia, An introduction to the singular value decomposition technique (SVD), in: Proceedings, 7th International Modal Analysis Conference, 1989, pp. 338–339.